


Variability of the Labrador Sea Surface Eddy Kinetic Energy Observed by Altimeter from 1993 to 2012

Weiwei Zhang^{1, 4}, and Xiao-Hai Yan¹⁻⁴ 

1. State Key Laboratory of Marine Environmental Science, Xiamen University, Xiamen, Fujian 361005, China

2. Laboratory for Regional Oceanography and Numerical Modeling, National Laboratory for Marine Science and Technology

3. College of Earth, Ocean, and Environment, University of Delaware, Newark, DE 19716

4. College of Ocean and Earth Sciences, Xiamen University, 4221 Xiang'An Nan Lu, Xiamen, Fujian 361102, China

Corresponding author: Xiao-Hai Yan, email: xiaohai@udel.edu

Key Points:

1. The Labrador Sea eddy kinetic energy shows strong interannual variability but no significant trend
2. Stronger eddy kinetic energy in the central Labrador Sea may be related to weaker restratification
3. The interannual variability may be driven by the North Atlantic Oscillation and the Subpolar Gyre circulation change

This article has been accepted for publication and undergone full peer review but has not been through the copyediting, typesetting, pagination and proofreading process which may lead to differences between this version and the Version of Record. Please cite this article as doi: 10.1002/2017JC013508

© 2018 American Geophysical Union

Received: Sep 28, 2017; Revised: Dec 11, 2017; Accepted: Dec 31, 2017

Abstract

A merged along track altimeter dataset is used to study the variability of eddy kinetic energy (EKE) in the Labrador Sea from 1993 to 2012. The EKE near the west Greenland current (WGC) has strong interannual variability without long-term trend from 1993 to 2012. The propagation direction of the Irminger Rings (IRs) originating from the WGC can be inferred from the EKE derived from altimeter, and the southward propagation of the IRs varies interannually. The central Labrador Sea EKE increases significantly from 1993 to 2012. The central Labrador Sea temperature difference between the end and the beginning of the winter convections is defined as restratification index to measure the restratification strengths. The relation between the central Labrador Sea EKE and the restratification index shows that the enhanced eddy activity originating from the west of the central Labrador Sea may cool the central Labrador Sea significantly. The interannual variability of the WGC EKE is likely to be driven by the large scale Subpolar Gyre (SPG) circulation variability and the North Atlantic Oscillation (NAO). The NAO also affects the central Labrador Sea EKE through its fingerprint in the local wind stress and surface heat flux. The NAO affects the WGC EKE by changing the SPG circulation strength, which will subsequently affect the WGC EKE through unknown physical processes.

1. Introduction

The Labrador Sea is an important area for global climate. The deep convection in the central Labrador Sea is the lower limb of the Atlantic Meridional Overturning Circulation (AMOC). As part of the Subpolar Gyre (SPG), the central Labrador Sea heat content is closely related to the SPG circulation (Häkkinen and Rhines, 2004), i.e. warmer central Labrador Sea corresponds to a weaker SPG. Recently, the Labrador Sea is identified as one of the locations subducting heat in the subsurface Atlantic, and contributing to the global warming hiatus (Meehl et al., 2011). The major heat sources for the central Labrador Sea is its boundary currents, injecting mesoscale eddies carrying the heat (Lilly et al., 2003; Katsman et al., 2004; Hátún et al., 2007; Gelderloos et al., 2011; Zhang and Yan, 2014).

According to origin, generation mechanisms, and structures, eddies in the Labrador Sea have been categorized into four types, the convective eddies, the boundary current eddies, the Irminger Rings (IRs), and the North Atlantic Current (NAC) eddies (Chanut et al. 2008; Luo et al. 2011; Gelderloos et al., 2011). The convective eddies and the radii of the background current eddies are from 5 to 15 km, and the radii of the IRs are observed to range from 15 km to 35 km (Prater et al., 2002; Lilly et al., 2003; Hátún et al., 2007). The IRs are triggered by strong topography gradient along the West Greenland continental shelf break, and initially they consist West Greenland Current (WGC) water in the surface layer, on top of the layer from the Irminger Currents, which they are named after (Katsman et al. 2004; Chanut et al., 2008). Idealized numerical studies have attempted to assess the thermal contributions by different types of eddies after convections (Jones and Marshall 1997; Katsman et al. 2004; Gelderloos et al., 2011), and

the IRs have been found to supply a significant amount of heat to the central Labrador Sea (Katsman et al., 2004; Gelderloos et al., 2011), which have not been confirmed by the realistic model configurations in the Labrador Sea (Luo et al., 2011; Zhang and Yan, 2014).

One cause of this discrepancy between realistic and idealized model is that the realistic models generate much fewer IRs propagating southward into the central Labrador Sea (Chanut et al., 2008; Luo et al., 2011; Zhang and Yan, 2014). Moreover, Lilly et al (2003) showed the altimeter-based eddy inventory during 1994-2000, and it can be inferred that about 60% to 70 % of the IRs propagate southward into the central Labrador Sea. This also results in much weaker EKE modeled in the central Labrador Sea (Luo et al., 2011).

Observations suggested that the seasonality of the WGC EKE is a consequence of basin-wide seasonal wind stress curl (Fischer et al., 2004; Brandt et al., 2004). However, it is not clear what is the driving process for the interannual variability of the WGC EKE, it can be local, such as central Labrador Sea convection and local wind forcing, or it can be driven by large scale circulations. Luo et al. (2011) were unable to reproduce the interannual variability of the WGC EKE even with monthly varying boundary condition and atmospheric forcing. Lilly et al. (2003) pointed out the decreasing number of eddies towards the end of the period 1994-2000, but cannot tell if it is due to weakened convection in the central Labrador Sea. Showing the EKE evolution after the deep convection in 1997, Brandt et al. (2004) speculated that the EKE may be enhanced after deep convection due to large heat content contrast between the interior and the boundary current of the Labrador Sea.

With more altimeter data available, it is possible for us to study the interannual variability of the Labrador Sea EKE, in terms of strengths and eddy propagations. It is also interesting to identify possible driving forces of the interannual variability, such as wind stress and large scale circulation. It is also important to clarify whether the convection events can affect the WGC EKE, and whether the WGC eddies can significantly contribute to the ocean heat content in the central Labrador Sea as predicted by simplified models.

The rest of this paper is organized as follows: section 2 provides details regarding the along track altimeter data processing, section 3 and 4 analyze the interannual EKE variability in the WGC area and the central Labrador Sea, and the EKE propagations from the WGC area to the central Labrador Sea. Section 5 and 6 investigate the interannual variability of other physical processes in the Labrador Sea and the SPG to investigate possible drivers for the interannual variability of the WGC EKE. Finally, section 7 summarizes and discusses the results.

2. Data and Methods

This study focuses on the long-term variability of EKE in the Labrador Sea, therefore, the Integrated Multi-Mission Altimeter Data for climate research (v2.0) is used. This SSH dataset integrated along track TOPEX/Poseidon altimeter data from cycle 1 to cycle 355, the cycle 13 to cycle 239 of Jason-1, and all the available Jason-2 cycles. The altimeter data are interpolated to a common reference orbit, with a 10-day repeat cycle. All inter-mission biases have been applied to provide a seamless transition throughout the two decades of data. Geophysical corrections, such as atmospheric and tidal corrections, have been applied to all the data. The data are downloaded from the Physical Oceanography

Distributed Active Archive Center (https://podaac.jpl.nasa.gov/Integrated_Multi-Mission_Ocean_AltimeterData). The data used in this study span from January 1993 to December 2012.

The data is further processed so that conspicuous spikes where along track sea level anomaly (SLA) gradient larger than 2.5 cm/km are removed, this criterion is the same as that chosen for the TOPEX/Poseidon data (Brandt et al. 2004). Afterwards, a 5-point hamming filter is applied to the despiked data. 3-, 7-, and 9-point hamming filters are also applied, and the 5-point hamming filter generates most reasonable result for the EKE field. The mean SSHA is removed at each sampling location on the referenced orbit before interpolated temporally to the mid-day of each month. For example, the 15th day or 14th day depending on the total number of days in that month, and the weighting function is the same as that used for the generation of the blended Sea Winds data by Zhang et al. (2006a, b):

$$W_k = \frac{2 - \frac{Dt^2}{T^2}}{2 + \frac{Dt^2}{T^2}}. \quad (1)$$

Here, Dt is the time interval between each along track sampling time and the mid-day of each month, and T is 15 or 14 days, again, depending on the number of days in that month. For each sampling location, only the observations within 15 days of the mid-day will be considered for the temporal interpolation. Since the along track satellite revisit time is about 10 days, each month there will be 0 to 3 samples available for the interpolation at each sampling location, the index k in equation (1) ranges from 0 to 3. Finally, the temporally interpolated data is mapped to 0.2° by 0.2° grid points, the

mapping methods are based on Gaussian weighting function and exponential smoothing function (Barnes 1994 a, b, c). The smoothing scale is 0.8 degree, similar to the cutoff scale chosen by Brandt et al. (2004).

To derive EKE from the processed SLA, the cross-track currents are estimated assuming geostrophic balance (Lilly et al., 2003):

$$v'_c \equiv \frac{g}{f} \frac{d\eta'}{dx_a}. \quad (2)$$

$\frac{d\eta'}{dx_a}$ is the along-track SLA gradient, g is gravitational acceleration, and f is the Coriolis parameter. Assuming the velocity anomaly v'_c is isotropic, then EKE can be defined as:

$$EKE \equiv \frac{1}{2} \overline{(u'^2 + v'^2)} = v_c'^2, \quad (3)$$

and furthermore, EKE can be represented by root-mean-square EKE speed denoted by

V_{EKE} :

$$V_{EKE} \equiv \sqrt{2v_c'^2}. \quad (4)$$

Empirical mode decomposition (EMD) method is a data-driven method for non-stationary data analysis, and its products are several fast or slow oscillating signals of different amplitude and frequency and a residual trend. An improved EMD, the complete ensemble EMD (CEEMD, Colominas et al., 2014), is used to decompose the data into intrinsic mode functions varies on different time scales, so physical processes can be compared on similar time scales. The residual of the CEEMD can also be interpreted as a nonlinear trend of the time series. Ezer and Corlett (2012) have identified a statistically significant nonlinear trend from the sea level anomaly observations, although no significant nonlinear trend has been identified.

The 0.25° Aviso delay time gridded SLA and corresponding geostrophic velocity anomaly datasets are used in this study. The data is interpolated to 1° grids for Empirical Orthogonal Function (EOF) analysis to be consistent with Hakkinen et al. (2004, 2013). The NCEP reanalysis 2 wind stress curl dataset is used to calculate the wind stress curl in the North Atlantic region. The latest monthly temperature and salinity data by European Centre for Medium Range Weather Forecasts Ocean Reanalysis System 4 (ORAS4) (Balmaseda et al., 2013) is used to represent the central Labrador Sea winter convection and restratification strengths.

3. Mean State and Seasonality of the EKE

The mean V_{EKE} from the merged along track altimeter is shown in figure 1a. Several locations show significant strong eddy activities. Notably, the high EKE originating from the vicinity of the WGC, the Labrador Current (LC), and the NAC. These high EKE locations have been identified by previous studies, and the magnitudes of the EKE speed in these areas are in line with previous studies (Prater, 2002; Lilly et al. 2003; Brandt et al. 2004). Another area of moderate EKE along the East Greenland Current is observed, and it has also been identified by numerical model study (Zhang and Yan, 2014). The EKE derived from the Aviso delayed time gridded sea level anomaly during the same time period also highlights the strong EKE in the WGC and NAC areas (Figure 1b). EKE in the WGC area spreads either southward or southwestward, indicating two pathways for eddy propagation. However, the EKE magnitude derived from the gridded altimeter data is much smaller than that derived from the along track altimeter and numerical models (Luo et al., 2011; Zhang and Yan, 2014). For instance, the magnitude of the WGC EKE from the along track altimeter is approximately twice of that from the gridded altimeter,

and the central Labrador Sea EKE is diminished in the gridded altimeter data (Figure 1b).

Furthermore, the EKE in Figure 1b does not capture the high EKE in the LC area, which has been revealed by the along track altimeter data (Prater 2002; Brandt et al., 2004) as well as high resolution numerical models (Luo et al., 2011; Zhang and Yan, 2014). Thus, the following study will focus on the EKE derived from the along track altimeter data.

Same as the study by Brandt et al. (2004), two regions in Figure 1a are chosen to show the interannual variability of the EKE, one in the West Greenland area ($60.5\text{--}64^{\circ}\text{N}$, $48\text{--}53^{\circ}\text{W}$), and the other in the central Labrador Sea ($56\text{--}59^{\circ}\text{N}$, $48\text{--}53^{\circ}\text{W}$). The mean EKE in the WGC area for the studied time period is $316\text{ cm}^2/\text{s}^2$, and $309\text{ cm}^2/\text{s}^2$ for the period 1993-2001, which is about $200\text{ cm}^2/\text{s}^2$ weaker than what was found by Brandt et al. (2004). The discrepancy is likely due to the different wavelengths for low pass filters applied to the along track altimeter data. Nevertheless, the interannual variability of the 6 months overlapping EKE in the WGC area (Figure 2a) is similar to that found by Brandt et al. (2004). For instance, the EKE is relatively low in 2000 and 2001, and it peaks between 1996 and 1997. The 20-year minimum is found around 2000. The mean EKE in the central Labrador Sea area (Figure 2b) is about $200\text{ cm}^2/\text{s}^2$, similar to the findings by Brandt et al. (2004). The time evolution of the number of eddies derived from the along track altimeter indicates that many mesoscale eddies, especially the anticyclonic and dipole ones, generated in the WGC area propagate southward into the central Labrador Sea (Lilly et al., 2003). On the other hand, the central Labrador Sea is also populated with convective and background eddies other than IRs. Here, the correlation coefficient between the EKE in the two regions from January to May is 0.51, above 95%

significance level. Thus, the activity of convective and background eddies have considerable contribution to the EKE in the central Labrador Sea.

Harmonic analysis shows that the maximum WGC EKE occurs mainly between 50 and 75 days of the year (Figure 2c), or mid-February to mid-March. This is consistent with previous study (Brandt et al., 2004). Except in 1997, the maximum EKE occurs quite early in January. The maximum EKE for the central Labrador Sea occurs mainly between 25 and 75 days (Figure 2d), which is similar to the results without correction associated with significant wave height (Brandt et al., 2004). The mean harmonic amplitude of the WGC EKE is about $100 \text{ cm}^2/\text{s}^2$, and about $55 \text{ cm}^2/\text{s}^2$ in the central Labrador Sea (Figure 2c, d). The harmonic amplitude of the WGC EKE become smaller after 2007, while it does not show similar decrease for the central Labrador Sea EKE.

The CEEMD method is applied to decompose the regional mean EKE data to identify statistically significant intrinsic modes, as well as to obtain the residual trend of the regional EKE. To test the significance of the decomposed intrinsic modes, the energy distributions are compared between the Gaussian distribution of white noise time series and the intrinsic modes (Wu and Huang, 2004). Significant interannual and annual modes are found for EKE in both the WGC (Figure 3a) and the central Labrador Sea area (Figure 4a). The significant modes of WGC EKE are comined (M2 and M3 in Figure 3a), and the amplitudes of the annual cycle also decreases after 2007, which is consistent with the harmonic analysis (Figure 2c). The combined M2 and M3 modes in figure 4a do not show long term changes of the amplitude of the annual cycle, but the strong interannual variability is similar to figure 2d. The EKE in the WGC and the central Labrador Sea do not show significant linear trend from 1993 to 2012. Here, using the CEEMD method, a

nonlinear trend can be derived as the residual of the decomposition. To test the robustness of the nonlinear trend, a bootstrap procedure is adopted following Ezer and Corlett (2012). It is found that the nonlinear trend of the WGC EKE does not reach the 95% confidence level (Figure 3c), so there is no longer change in the WGC EKE. The central Labrador Sea EKE, however, is significantly enhanced after 2003 (Figure 4c). The EKE activity in the central Labrador Sea has a strong implication on the heat transport from the boundary currents, and its enhancement is believed to result in more rapid warming of the central Labrador Sea (Katsman et al. 2004, Gelderloos et al., 2011).

4. EKE Propagation

Not only the area of high EKE originating from the WGC varies, but also the shape of the high EKE area or the directions to which the high EKE area spreads into the Labrador Sea interior varies interannually. The spreading direction of the high EKE area from the WGC can implicate the generation and propagation direction of the mesoscale eddies in this area, namely the IRs (Prater 2002; Lilly et al. 2003; Hátún et al. 2007; Chanut et al. 2008), which have been found to be active and efficient in restratifying the convection area in the central Labrador Sea (Katsman et al. 2004; Hátún et al. 2007; Gelderloos et al. 2011; Zhang and Yan, 2014). Both westward and southward evolution of high EKE from the WGC are shown in figure 5.

The latitude-time diagram of EKE between 48°W and 56°W is shown from 1993 to 2012 (Figure 5a). The magnitude of WGC EKE propagating into the central Labrador Sea (south of 59.5°N) shows strong interannual variability. Since the WGC EKE is mainly contributed due to the mesoscale IRs, higher EKE reaching 59.5°N indicates more IRs entering the central Labrador Sea. The WGC EKE is larger than $400 \text{ cm}^2/\text{s}^2$ at 59.5°N in

certain years, such as 1997-1999, 2003, and 2007. During these years, the winter EKE in the WGC are also much stronger. The mean propagation speed of EKE in these years is about 4.5 cm/s, in line with previous studies (Lilly et al., 2003; Brandt et al., 2004). The EKE is also larger than $400 \text{ cm}^2/\text{s}^2$ at 59.5°N in 1994, but the southward increase is much faster than the interior drifting speed, the increase of EKE is more likely to be simultaneous between 58.5°N and 61.5°N . After 2001, the EKE is stronger south of 59°N . Since the convection in the central Labrador Sea is weakened from 1998 to 2012, except in early 2008 (Våge et al., 2009), convective eddies are not likely to cause the increase. The WGC EKE increases from 1999-2005 (Figure 3c), given the typical life time of IRs of 6 months to 1 year (Lilly et al., 2003; Chanut et al., 2008), it is unlikely that more IRs enter the central Labrador Sea and cause the EKE increase after 2001 (Figure 4c, 5a). Therefore, the boundary current eddies present all year around may have contributed to the EKE increase. The westward EKE propagation of the EKE is also around 5 cm/s (Figure 5b). The expansion extents towards south and west are consistent during years 1997-1999, 2003 and 2007.

Hátún et al. (2007) tracked three anticyclonic IRs that propagate westward at a speed of 15 cm/s. Hydrographic data also indicates that the IRs propagates faster (12-20 cm/s) along the westward pathway, which is roughly along the 3000 m isobaths (Rykova et al., 2009). The discrepancy can be due to the following reasons: firstly the EKE propagation speed is more like the group speed of eddies, so it is slower than some eddies; secondly, the propagation speed derived from EKE expansion is from Eulerian perspective, while the propagation speed derived by Hátún et al. (2007) is of Lagrangian perspective.

5. Impact on the Central Labrador Sea

The eddy activity in WGC and central Labrador Sea may have a strong influence on the deep convection and restratification. To quantitatively investigate these relations, both the deep convection and restratification are measured using physical parameters derived from the ORAs4 dataset: the mixed layer depth and the heat content regain after convection. The ORAs4 mean potential temperature and salinity evolution in the central Labrador Sea within the rectangular box in figure 1a are shown in figure 6, and the reanalysis data show similar evolution patterns to that derived from the Argo floats data during 1996-2000 (Straneo, 2006) and 2003-2012 (Kieke and Yashayaev, 2015).

Brandt et al. (2004) found strong and continuous EKE generation in the WGC area and almost simultaneous EKE increase in the central Labrador Sea after the moderate convection in 1997 (Pickart et al., 2002), and speculated that the strong convections from 1994-1996 may have increased the heat content contrast between boundary currents and the central Labrador Sea, hence the WGC was strengthened. The mean mixed layer depth in winter months within the rectangular box is chosen to represent the convection strength (Figure 7a), since Lavender et al. (2002) found deep convections mostly occur here. Here, it shows that the wintertime mixed layer depth derived from ORAs4 is not significantly correlated with the WGC EKE or the central Labrador Sea EKE. Moreover, the regression of the WGC EKE on the WGC does not show significant correlation either (no shown). Here, the WGC is the Aviso gridded sea surface absolute geostrophic velocities derived from the absolute dynamic topography.

Since the winter convection is usually strongest from January to March, the so called restratification begins after March. During the restratification the central Labrador Sea ocean heat content increases from April to December. The regained heat after convection

mainly comes from the eddy heat flux at depths below 200 meters, where surface heat flux is unlikely to contribute (Straneo, 2006; Zhang and Yan 2014). Therefore, the heat content increase from April to December below 200 meters is a reasonable index for the restratification strengths. Thus the 200 to 1000 m mean temperature difference between December and April can be defined as the restratification index.

Idealized numerical model showed that the IRs generated at the WGC area can effectively boost the restratification process and can shorten the time required for restratification (Gelderloos et al., 2011). Although the EKE in the WGC and the central Labrador Sea are significantly correlated, indicating that significant amount of IRs can propagate in to the central Labrador Sea, the WGC EKE does not significantly correlate with the restratification index. On the other hand, the correlation coefficient between the central Labrador Sea EKE and the restratification index is -0.69, and is above the 95% confidence level. The evolution of the restratification index and the central Labrador Sea EKE from April to December is shown in figure 7b. In the central Labrador Sea, the eddies of all sizes are supposed to bring heat from the boundary currents (Straneo, 2006; Gelderloos et al., 2011), so intuitively, higher EKE level should result in more effective restratification. However, the correlation coefficient indicates the opposite.

The eddies presented in the central Labrador Sea can be convective eddies, the IRs, and the background eddies (Chanut et al., 2008; Gelderloos et al., 2011). Convective eddies are less active in most of the studies years, due to weakened convection activity after 1996. The IRs originating from the WGC area carry warmer water from the Irminger Current (Gelderloos et al., 2011; Hátún et al., 2007), so if the increasing central Labrador Sea EKE is due to more IRs, then the restratification should strengthen. Thus,

the negative correlation coefficient between EKE and restratification index (figure 7b) indicates that some background eddies can bring colder water into the central Labrador Sea. The mean potential temperature within the 200-1000 meter layer from 1993-2012 is colder to the west and south of the Labrador Sea box (Figure 8), so it is possible that more background eddies are generated locally at the west and south of the central Labrador Sea, and they cause more heat exchange with the colder waters. Negative eddy advection of heat has been identified between 1000 and 3000 isobaths to the west and south of the box by Seanko et al. (2014).

6. Possible Drivers for the EKE Interannual Variability

Häkkinen and Rhines (2004) have shown that the first principle component (PC) of the SLA in the North Atlantic can represent the SPG interannual variability, thus it can be designated as a SPG index. The SPG index can represent both the overall SPG circulation flow strength as well as the SPG interior ocean heat content (Häkkinen and Rhines , 2004; Häkkinen et al., 2013). Similarly, the empirical orthogonal function analysis is applied to the Aviso 0.25° by 0.25° delayed time SLA, and the PC1 and corresponding EOF1 is shown in figure 9. The time series of the PC1 or the SPG index decreases meaning that the SPG has been weakening significantly during the study period (Figure 9a). The negative SLA within the SPG results in the counterclockwise SPG circulation, which has been weakening during the study period as shown by the nonlinear trend from the CEEMD residual (Figure 9a). The SPG index is then detrended by removing the nonlinear CEEMD residual from the original time series. The detrended SPG index from September to November agrees well with the December to March NAO index: stronger during positive NAO phase, and vice versa. The correlation coefficient between the two

is 0.73 above 95% confidence level. The interannual variability of the subpolar North Atlantic heat content is largely driven by the surface wind forcing and heat flux associated with NAO, and NAO positive will result in a colder SPG in general (Lozier 2008). Since the sea level anomaly is highly affected by the ocean heat content through thermal expansion, a colder SPG also means a stronger SPG (Häkkinen and Rhines, 2004).

Both the NAO index and the SPG index are significantly correlated with the WGC EKE (Figure 10). The one-year lag correlation coefficient between December to March NAO index and the January to May mean WGC EKE is -0.53 above 95% confidence level, with the NAO leading the WGC EKE. The correlation coefficients between the September to November SPG index and the following January to May WGC EKE is -0.48. The time series of the WGC EKE closely follows the SPG index, except in 1993 and 2007, when the WGC EKE is extremely strong. Based on the linear regression analysis, it is possible that the December to March atmospheric forcing sets the ocean circulation as well as the ocean heat content later from September to November, which will have a significant effect on the following year's winter and spring EKE in the WGC area.

It has been demonstrated that the WGC EKE may be driven by the interannual variability of the NAO and the SPG circulation. Other than the large scale circulations, local wind stress may also affect the Labrador Sea EKE. The local wind stress curl annual cycle has been found to be in phase with that of the WGC EKE (Brandt et al., 2004), but it is not known whether it drives the interannual variability of the WGC EKE as well. Luo et al. (2011) have attempted to find whether the interannually varying wind

forcing or boundary current drives the WGC EKE interannual variability, but the modeled WGC EKE did not compare well with the observed EKE. Moreover, their modeled EKE has a much weaker annual cycle than altimeter observation.

Here, the NCEP reanalysis 2 momentum flux is used to derive the January to May wind stress curl in the study area, and its correlation coefficient with the time series of the regional mean EKE in the WGC and the central Labrador is presented (Figure 11). The correlation coefficient in figure 11a indicates that the WGC EKE is not likely to be directly driven by the local wind stress forcing in the Labrador Sea. While the central Labrador Sea EKE is highly responsive to the local wind stress forcing (Figure 11b). Stronger local wind stress will induce more heat loss in the central Labrador Sea, which will strengthen the convection and generate more convective eddies (Jones and Marshall, 1997).

7. Summary and Discussion

This study used the along track Integrated Multi-Mission Altimeter Data for climate research (v2.0) from 1993 to 2012 in the Labrador Sea, where deep convection occurs in the central basin as an important component of the AMOC. The EKE is inferred from the cross track SLA gradient. The EKE is strongest in the WGC area, and then extends southward and westward into the central Labrador Sea (Figure 1a). Thus, the propagation and strengths of the WGC EKE may have an important implication on the heat content variability of the central Labrador Sea.

During the study period, the WGC EKE shows strong interannual variability, but did not show significant long-term linear or nonlinear trend (Figure 3c). The central Labrador Sea EKE is significantly correlated with the WGC EKE, but unlike the WGC EKE, it

significantly increases after 2003 (Figure 4c) possibly due to enhanced boundary current eddy activity given the weakening convections. Moreover, the propagation speed of the WGC EKE has strong interannual variability, and the significant southward propagation only occurs when the WGC EKE is very strong, such as in 1997-1999, 2003-2005, and 2007. When assessing the performance of the numerical models in the Labrador Sea (Chanut et al., 2008; Luo et al., 2011; Zhang and Yan, 2014), the simulated weak EKE in the central Labrador Sea may not be attributed to that the modeled IRs fail to propagate into it.

Although the WGC EKE is significantly correlated with the central Labrador Sea EKE possibly due to the IRs southward propagation, the WGC EKE is not significantly correlated with the convection strength in the central Labrador Sea. Brandt et al. (2004) have speculated that after years of deep convection, the enhanced boundary-interior heat contrast may boost the WGC EKE. This cannot be corroborated by this study, since there has been no continuous deep convection since 1994-1996. Furthermore, the WGC EKE did not increase after the 2008 deep convection (Våge et al., 2009; Zhang and Yan, 2014). No significant correlation has been found between the WGC EKE and the mixed layer depths during 1993-2012, but it should be noted that the deepest convection sites may change in some years, which is not presented in the low resolution ORAs4 dataset. Indeed, Våge et al. (2009) used Argo profiles data and found deeper convections occur in 2008 to the northwest of the rectangular box in figure 1a.

A restratification index is proposed using the ORAs4 reanalysis data. It has been shown that stronger central Labrador Sea EKE is negatively correlated with the restratification strength (Figure 7b). The counterintuitive result is likely due to enhanced

local eddy activity in the west and south of the central Labrador Sea, and these eddies may have enhanced the heat exchange between the central Labrador Sea and the colder ambient water to its west and south (Figure 8). Yet, it should be noted other mechanisms may have caused both the EKE increase and restratification weakening in the central Labrador Sea. The central Labrador Sea EKE is significantly correlated with the local wind stress changes (Figure 11b). The interannual variability of the WGC EKE may be driven by the previous winter heat flux and wind stress anomaly associated with the NAO index and subsequent SPG circulation changes. However, it is not clear what exactly are the processes for the SPG circulation, such as the sea surface anomaly and current system in the upper 1000 meter, to act on the WGC EKE generation. Thus, High resolution numerical model may be able to unravel this problem by analyzing the EKE source and sinks related to different aspects of the SPG circulation.

Acknowledgement:

We thank the China Postdoctoral Science Foundation (2017M612125), SOA Global Change and Air-Sea Interaction Project (GASI-IPOVAI-01-04), National Natural Science Foundation of China (41630963, 41476007), and the State Key Laboratory of Marine Environmental Science Postdoctoral Fellowship for financial support. The along-track altimeter data is obtained from Physical Oceanography Distributed Active Archive Center (https://podaac.jpl.nasa.gov/Integrated_Multi-Mission_Ocean_AltimeterData).

ORAs4 reanalysis data is generated by European Center for Mid-Range Weather Forecasting and available for public (http://icdc.zmaw.de/easy_init_ocean.html?&L=1).

The gridded sea surface absolute dynamic topography and corresponding geostrophic current data is produced by Aviso, and is available at Copernicus Marine and Environment Monitoring Service (<http://marine.copernicus.eu/services-portfolio/access-to-products>). The NCEP Reanalysis 2 is downloaded from the Earth System Research Laboratory (<https://www.esrl.noaa.gov/psd/data/gridded/data.ncep.reanalysis2.html>).

References:

- Balmaseda, M. A., K. Mogensen, and A. T. Weaver (2013), Evaluation of the ECMWF ocean reanalysis system ORAS4, *Q. J. R. Meteorol. Soc.*, *139*, 1132-1161.
- Barnes, S. (1994), Applications of the Barnes Objective Analysis Scheme .1. Effects of Undersampling, Wave Position, and Station Randomness, *J. Atmos. Ocean. Technol.*, *11*, 1433-1448.
- Barnes, S. (1994), Applications of the Barnes Objective Analysis Scheme .2. Improving Derivative Estimates, *J. Atmos. Ocean. Technol.*, *11*, 1449-1458.
- Barnes, S. (1994), Applications of the Barnes Objective Analysis Scheme .3. Tuning for Minimum Error, *J. Atmos. Ocean. Technol.*, *11*, 1459-1479.
- Brandt, P., F. Schott, A. Funk, and C. Martins (2004), Seasonal to interannual variability of the eddy field in the Labrador Sea from satellite altimetry, *J. Geophys. Res. - Oceans*, *109*, C02028.
- Chanut, J., B. Barnier, W. Large, L. Debreu, T. Penduff, J. M. Molines, and P. Mathiot (2008), Mesoscale eddies in the Labrador Sea and their contribution to convection and restratification, *J. Phys. Oceanogr.*, *38*, 1617-1643.
- Colominas, M. A., G. Schlotthauer, and M. E. Torres (2014), Improved complete ensemble EMD: A suitable tool for biomedical signal processing, *Biomedical Signal Processing and Control*, *14*, 19-29.

Ezer, T. and W. B. Corlett (2012), Is sea level rise accelerating in the Chesapeake Bay?

A demonstration of a novel new approach for analyzing sea level data, *Geophys. Res. Lett.*, *39*, doi: 10.1029/2012GL053435.

Gelderloos, R., C. A. Katsman, and S. S. Drijfhout (2011), Assessing the Roles of Three

Eddy Types in Restratifying the Labrador Sea after Deep Convection, *J. Phys. Oceanogr.*, *41*, 2102-2119.

Gelderloos, R., F. Straneo, and C. A. Katsman (2012), Mechanisms behind the

Temporary Shutdown of Deep Convection in the Labrador Sea: Lessons from the Great Salinity Anomaly Years 1968-71, *J. Clim.*, *25*, 6743-6755.

Fischer, J., F. A. Schott, and M. Dengler (2004), Boundary circulation at the exit of the

Labrador Sea, *J. Phys. Oceanogr.*, *34*, 1548-1570.

Häkkinen, S. and P. Rhines (2004), Decline of subpolar North Atlantic circulation during

the 1990s, *Science*, *304*, 555-559.

Häkkinen, S., P. B. Rhines, and D. L. Worthen (2011), Atmospheric Blocking and

Atlantic Multidecadal Ocean Variability, *Science*, *334*, 655-659.

Häkkinen, S., P. B. Rhines, and D. L. Worthen (2013), Northern North Atlantic sea

surface height and ocean heat content variability, *Journal of Geophysical Research-Oceans*, *118*, 3670-3678.

Hátún, H., C. C. Eriksen, and P. B. Rhines (2007), Buoyant eddies entering the Labrador

Sea observed with gliders and altimetry, *J. Phys. Oceanogr.*, *37*, 2838-2854.

Katsman, C., M. Spall, and R. Pickart (2004), Boundary current eddies and their role in the restratification of the Labrador Sea, *J. Phys. Oceanogr.*, *34*, 1967-1983.

Kieke, D. and I. Yashayaev (2015), Studies of Labrador Sea Water formation and variability in the subpolar North Atlantic in the light of international partnership and collaboration, *Prog. Oceanogr.*, *132*, 220-232.

Lavender, K.L., R.E. Davis, and W. B. Owens (2002), Observations of Open-Ocean Deep Convection in the Labrador Sea from Subsurface Floats, *J. Phys. Oceanogr.*, *32*, 511-526.

Lazier, J., R. Hendry, A. Clarke, I. Yashayaev, and P. Rhines (2002), Convection and restratification in the Labrador Sea, 1990-2000, *Deep-Sea Res. I*, *49*, 1819-1835.

Lilly, J., P. Rhines, F. Schott, K. Lavender, J. Lazier, U. Send, and E. D'Asaro (2003), Observations of the Labrador Sea eddy field, *Prog. Oceanogr.*, *59*, 75-176.

Luo, H., A. Bracco, and E. Di Lorenzo (2011), The interannual variability of the surface eddy kinetic energy in the Labrador Sea, *Prog. Oceanogr.*, *91*, 295-311.

Luo, H., A. Bracco, and F. Zhang (2014), The Seasonality of Convective Events in the Labrador Sea, *J. Clim.*, *27*, 6456-6471.

Lozier, M.S., S.J. Leadbetter, R.G. Williams, V. Roussenov, M.S.C. Reed and N.J. Moore (2008), The spatial pattern and mechanisms of heat content change in the North Atlantic. *Science*, *319*, 800-803.

- Meehl, G. A., J. M. Arblaster, J. T. Fasullo, A. Hu, and K. E. Trenberth (2011), Model-based evidence of deep-ocean heat uptake during surface-temperature hiatus periods, *Nat. Clim. Chang.*, *1*, 360-364.
- Pickart, R. S., D. J. Torres, and R. A. Clarke (2002), Hydrography of the Labrador Sea during active convection, *J. Phys. Oceanogr.*, *32*, 428-457.
- Prater, M. (2002), Eddies in the Labrador Sea as observed by profiling RAFOS floats and remote sensing, *J. Phys. Oceanogr.*, *32*, 411-427.
- Rykova, T., F. Straneo, J. M. Lilly, and I. Yashayaev (2009), Irminger Current anticyclones in the Labrador Sea observed in the hydrographic record, 1990-2004, *J. Mar. Res.*, *67*, 361-384.
- Seanko, O.A., F. Dupont, D. Yang, P.G. Mayers, I. Yashayev, and G.C. Smith (2014), Role of resolved and parameterized eddies in the Labrador Sea Balance of Heat and Bouyancy, *J. Phys. Oceanogr.*, *44*, 3008-3032.
- Straneo, F. (2006), Heat and freshwater transport through the central Labrador Sea, *J. Phys. Oceanogr.*, *36*, 606-628.
- The Lab Sea Group (1998), The Labrador Sea deep convection experiment, *Bull. Amer. Meteor.*, *79*, 2033-2058.
- Våge, K. et al. (2009), Surprising return of deep convection to the subpolar North Atlantic Ocean in winter 2007-2008, *Nat. Geosci.*, *2*, 67-72.

Wu, Z. and N. E. Huang (2004), A study of the characteristics of white noise using empirical mode decomposition method, *Proc. R. Soc. Lond. A*, 460, 1597-1611.

Yashayaev, I. and J. W. Loder (2009), Enhanced production of Labrador Sea water in 2008, *Geophys. Res. Lett.*, 36, L01606.

Zhang, H., J. J. Bates, and R. W. Reynolds (2006), Assessment of composite global sampling: Sea surface wind speed, *Geophys. Res. Lett.*, 33, L17714.

Zhang, W. and X. Yan (2014), Lateral heat exchange after the Labrador Sea deep convection in 2008, *J. Phys. Oceanogr.*, 44, 2991-3007.

Figure Captions:

Figure 1. The mean root-mean-square EKE velocity (unit: cm s^{-1}) from January 1993 to December 2012. (a) is derived from the merged along track altimeter data, see text for processing details, and (b) is derived from the delayed time all-satellite merged sea level anomalies provided by Aviso. The areas within the triangle and the rectangle are designated as the Northern Labrador Sea and the Central Labrador Sea.

Figure 2. The evolution of regional mean EKE (unit: cm^2/s^2) in (a) the northern Labrador Sea and (b) central Labrador Sea. The regions are the boxes in Fig. 1, and the choices are similar to Brandt et al. (2004). The black curves are the monthly EKE with scales on the left, while the grey curves are the 6 months overlapping annual mean EKE with grey scales on the right. (c) The annual harmonic amplitude (cm^2/s^2) and phase (unit: days) of EKE for the northern Labrador Sea, and (d) is the same but for the central Labrador Sea.

Figure 3. The time series of the decomposed WGC EKE using CEEMD. (a) The combined interannual mode 2 and mode 3, which are significantly different from white noise as M2 and M3 shown in (b). The grey solid and dashed lines in (b) are the limits for 99 % and 95% confidence level. (c) shows the significance test for the residual nonlinear trend of the WGC EKE. The solid black line is the nonlinear trend as residual from CEEMD analysis of the WGC EKE. The thick solid grey line is the mean trend of the bootstrap samples, the dashed thick grey lines are the 95% confidence interval for the nonlinear trend, and the solid thin grey lines are the one standard deviation for the bootstrap samples.

Figure 4. Figure 4. Same as figure 3, but for the central Labrador Sea area. Notice it is also the M2 and M3 modes on interannual time scales that are significant.

Figure 5. The time evolution of (a) zonal mean EKE from 48°W to 54°W, and (b) the meridional mean EKE from 59.5°N to 62.5°N. The dashed white lines indicate the propagation of EKE, and the solid white line indicates the 59.5°N latitude.

Figure 6. The evolution of the mean potential temperature (a) and salinity (b) in the central Labrador Sea within 3250 m isobath, as defined by Yashayaev and Loder (2009), note that the salinity color is not linearly scaled. The time-axis ticks represent the beginning of each year.

Figure 7. (a) Time series of the mean mixed layer depth in January to March in the central Labrador Sea within the rectangular box in figure 1a. The mixed layer is defined as the depth where the potential density exceeds the surface value by 0.01 kg/m³ (Lazier et al., 2002). (b) The thin line is the time series of the difference between December and March mean temperature at 200-1000 m, and the thick line is the mean central Labrador Sea EKE from April to December.

Figure 8. The ORAs4 mean potential temperature within the 200-1000 m layer from 1993 to 2012. The black box is the same as in figure 1a.

Figure 9. The subpolar gyre index: (a) The time series of the PC1 of the Aviso sea level anomalies (thin curve), and the time series with its nonlinear trend (dashed curve)

removed (thick curve), overlapped by NAO index from December to March (grey bars) (a) and the associated EOF1 on $1^\circ \times 1^\circ$ grids (b).

Figure 10. Time evolution from 1993 to 2012 for the normalized WGC EKE (black curve, unit: cm^2/s^2), the nonlinearly detrended and normalized September to December SPG index timed by -100 (grey curve), and the December to March NAO index timed by 30 (grey bars).

Figure 11. The correlation coefficient of (a) the WGC EKE and (b) the central Labrador Sea EKE from January to May with the NCEP reanalysis2 annual wind stress curl averaged from January to May. The stippling indicates confidence level above 95%.

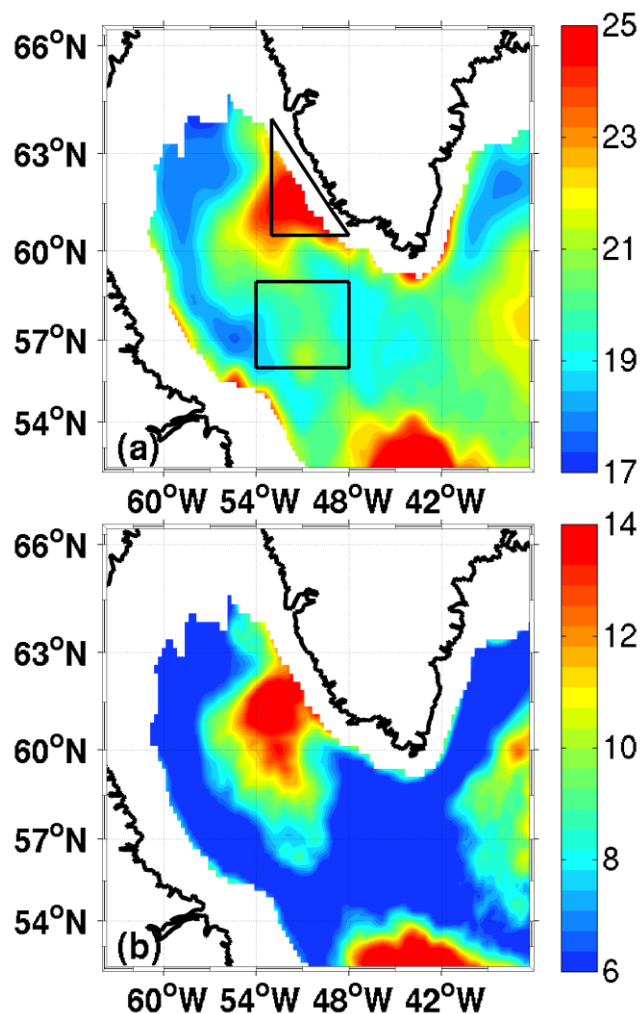


Figure 1. The mean root-mean-square EKE velocity (unit: cm s^{-1} from January 1993 to December 2012. (a) is derived from the merged along track altimeter data, see text for processing details, and (b) is derived from the delayed time all-satellite merged sea level anomalies provided by Aviso. The areas within the triangle and the rectangle are designated as the Northern Labrador Sea and the Central Labrador Sea.

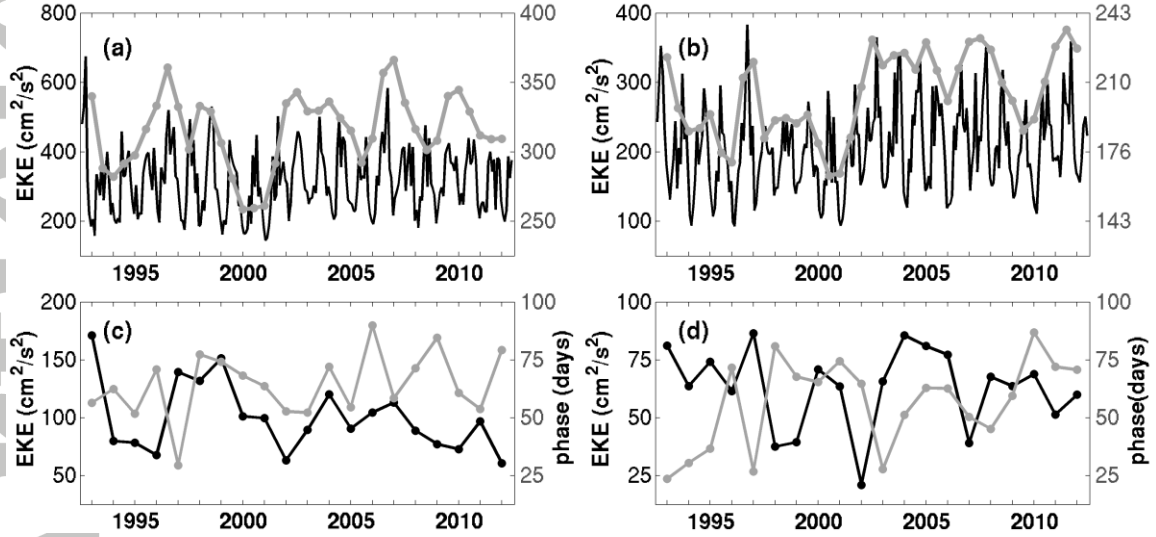


Figure 2. The evolution of regional mean EKE (unit: cm^2/s^2) in (a) the northern Labrador Sea and (b) central Labrador Sea. The regions are the boxes in Fig. 1, and the choices are the same as these by Brandt et al. (2004). The black curves are the monthly EKE with scales on the left, while the grey curves are the 6 months overlapping annual mean EKE with grey scales on the right. (c) The annual harmonic amplitude (cm^2/s^2) and phase (unit: days) of EKE for the northern Labrador Sea, and (d) is the same but for the central Labrador Sea.

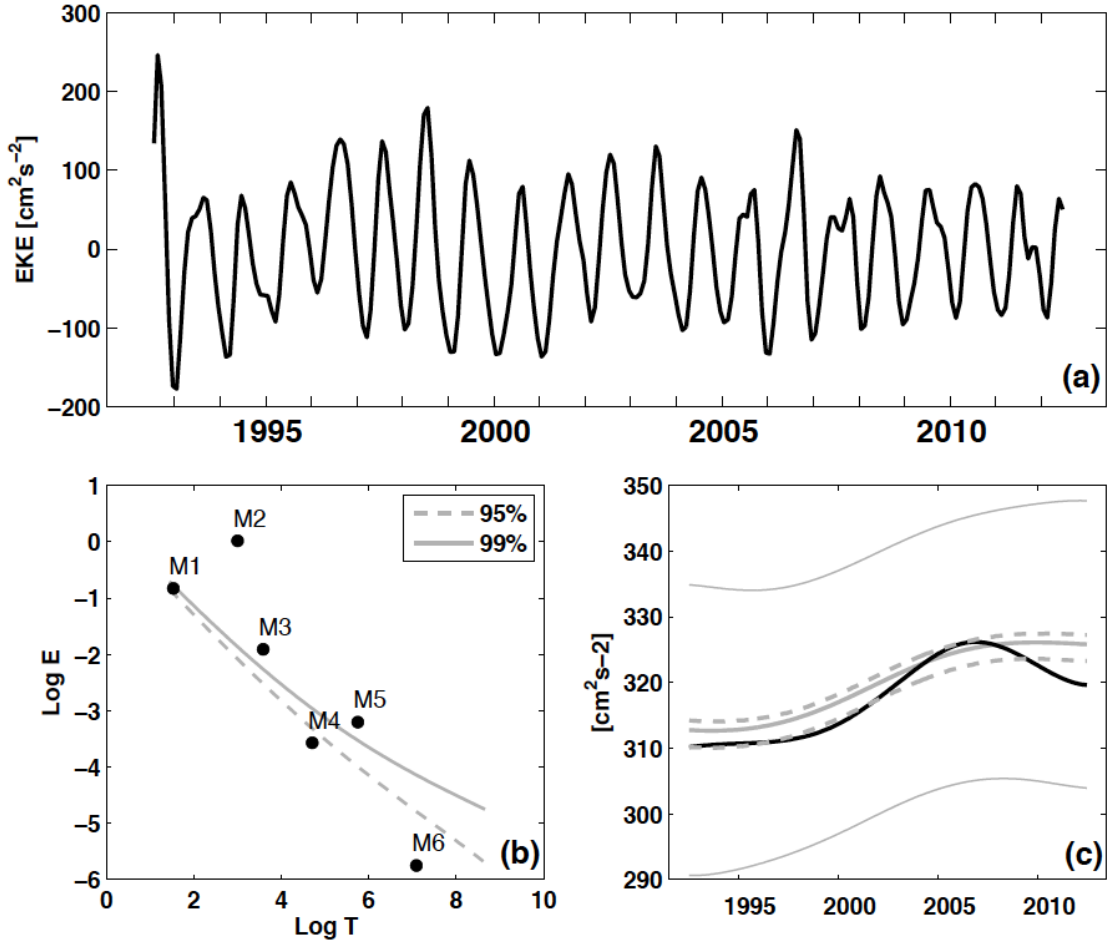


Figure 3. The time series of the decomposed WGC EKE using CEEMD. (a) The combined interannual mode 2 and mode 3, which are significantly different from white noise as M2 and M3 shown in (b). The grey solid and dashed lines in (b) are the limits for 99 % and 95% confidence level. (c) shows the significance test for the residual nonlinear trend of the WGC EKE. The solid black line is the nonlinear trend as residual from CEEMD analysis of the WGC EKE. The thick solid grey line is the mean trend of the bootstrap samples, the dashed thick grey lines are the 95% confidence interval for the nonlinear trend, and the solid thin grey lines are the one standard deviation for the bootstrap samples.

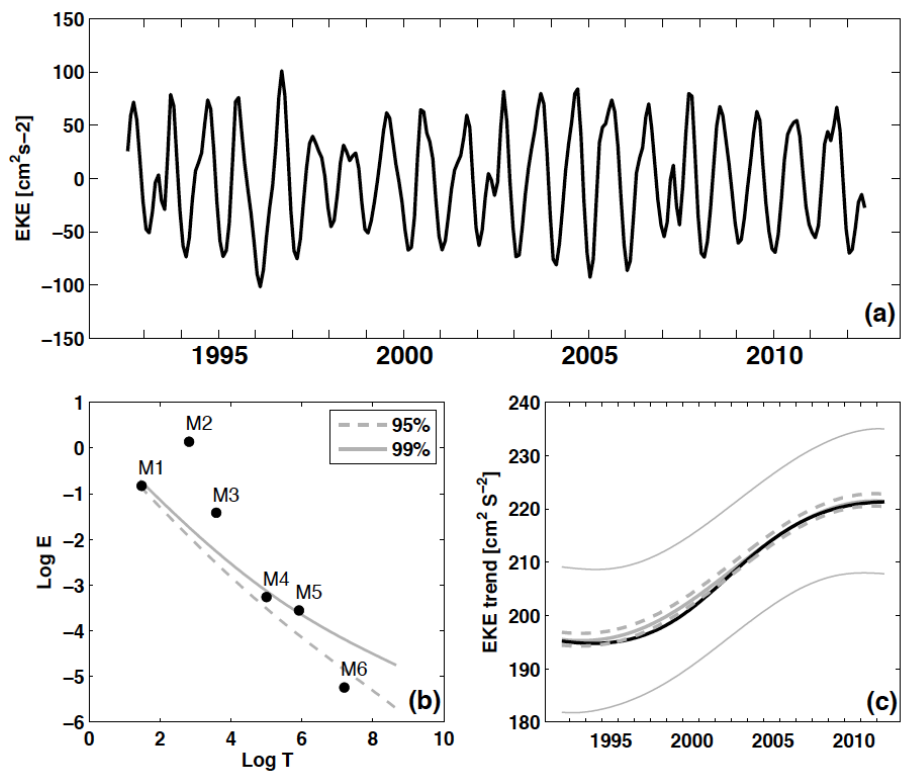


Figure 4. Same as figure 3, but for the central Labrador Sea area. Notice it is also the M2 and M3 modes on interannual time scales that are significant.

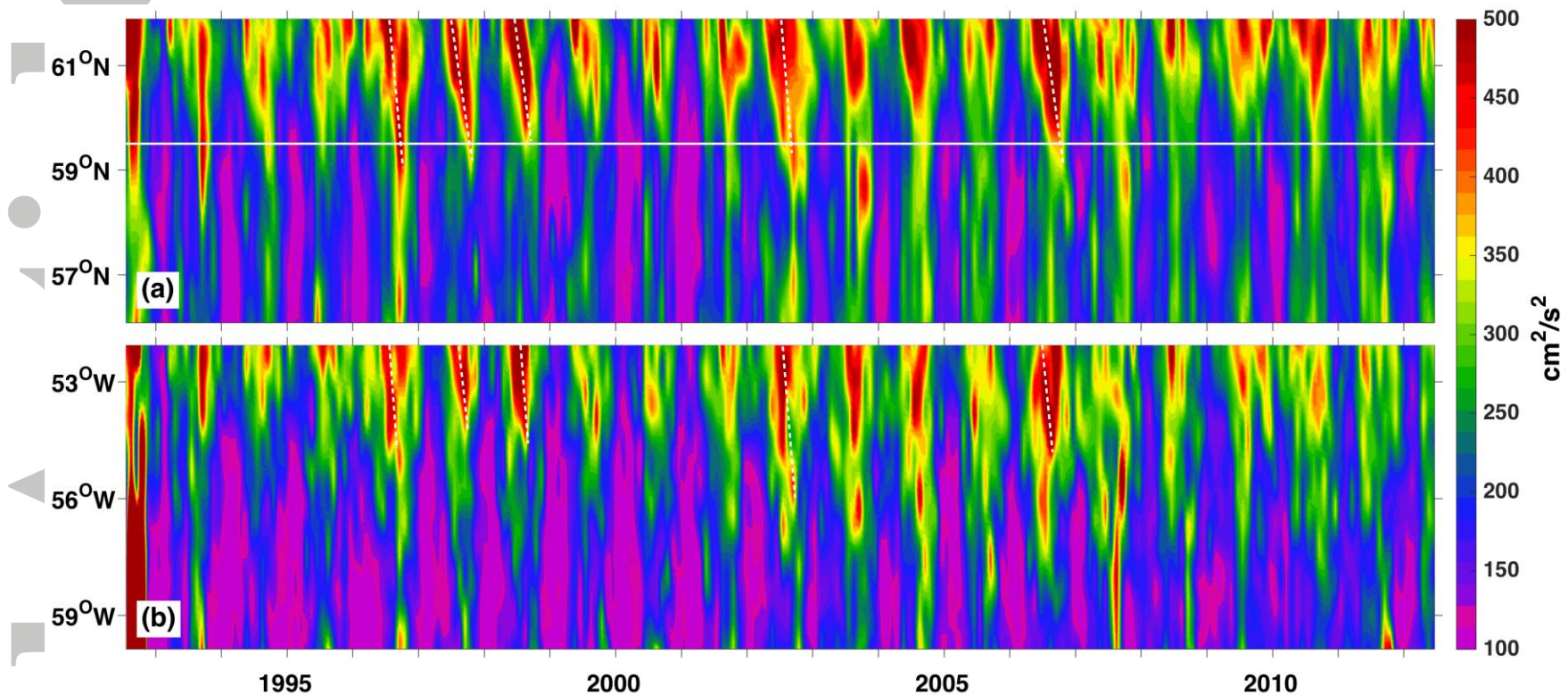


Figure 5. The time evolution of (a) zonal mean EKE from 48°W to 54°W , and (b) the meridional mean EKE from 59.5°N to 62.5°N . The dashed white lines indicate the propagation of EKE, and the solid white line indicates the 59.5°N latitude.

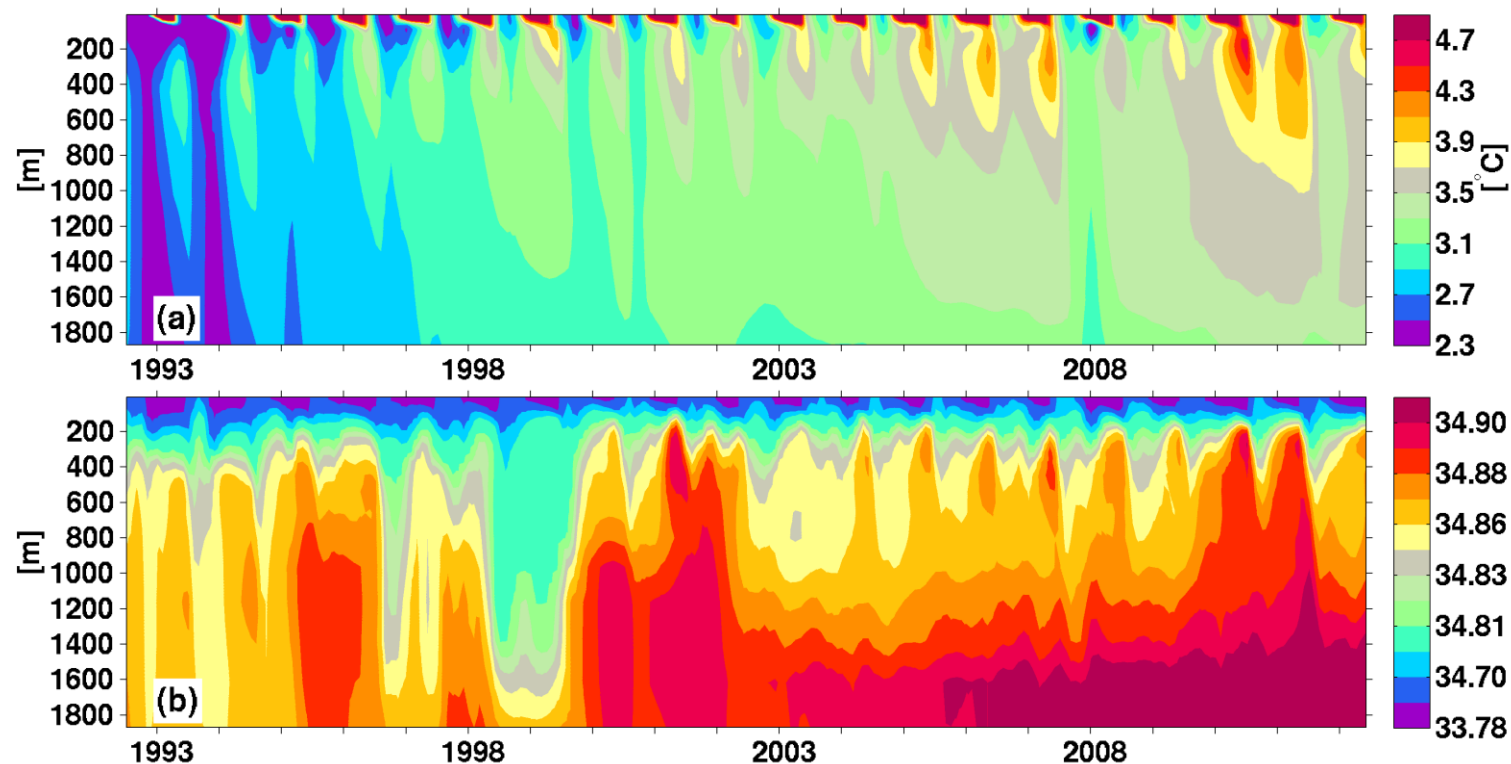


Figure 6. The evolution of the mean potential temperature (a) and salinity (b) in the central Labrador Sea within 3250 m isobath, as defined by Yashayaev and Loder (2009), note that the salinity color is not linearly scaled. The time-axis ticks represent the beginning of each year.

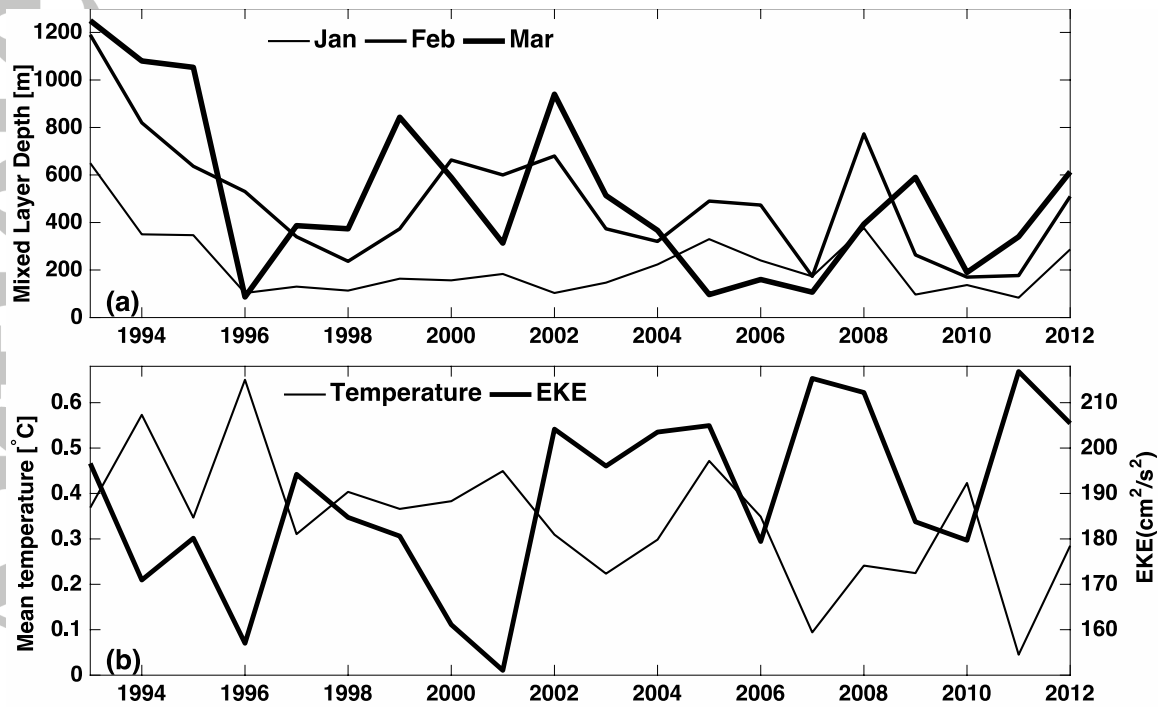


Figure 7. (a) Time series of the mean mixed layer depth in January to March in the central Labrador Sea within the rectangular box in figure 1a. The mixed layer is defined as the depth where the potential density exceeds the surface value by 0.01 kg/m^3 (Lazier et al., 2002). (b) The thin line is the time series of the difference between December and March mean temperature at 200-1000 m, and the thick line is the mean central Labrador Sea EKE from April to December.

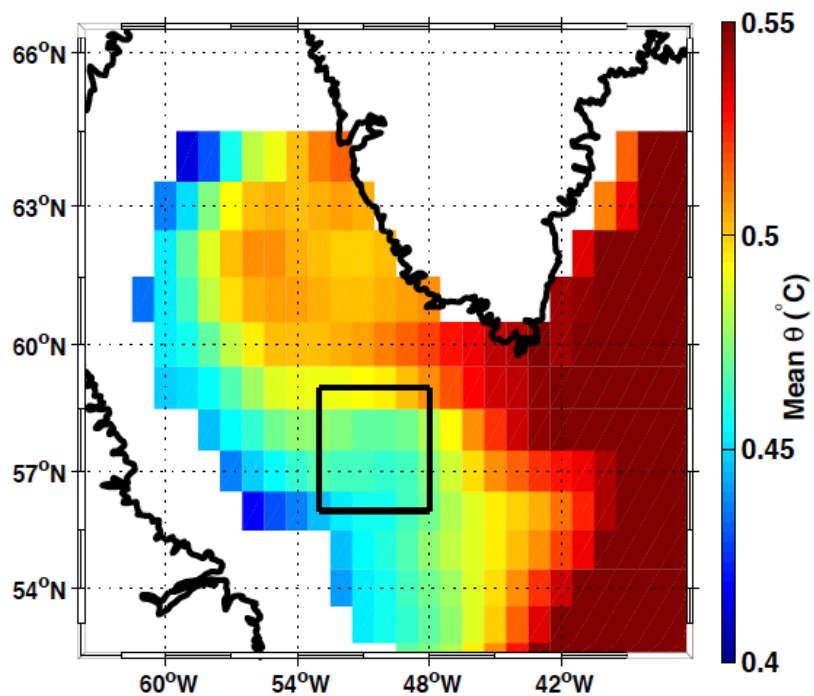


Figure 8. The ORAs4 mean potential temperature within the 200-1000 m layer from 1993 to 2012. The black box is the same as in figure 1a.

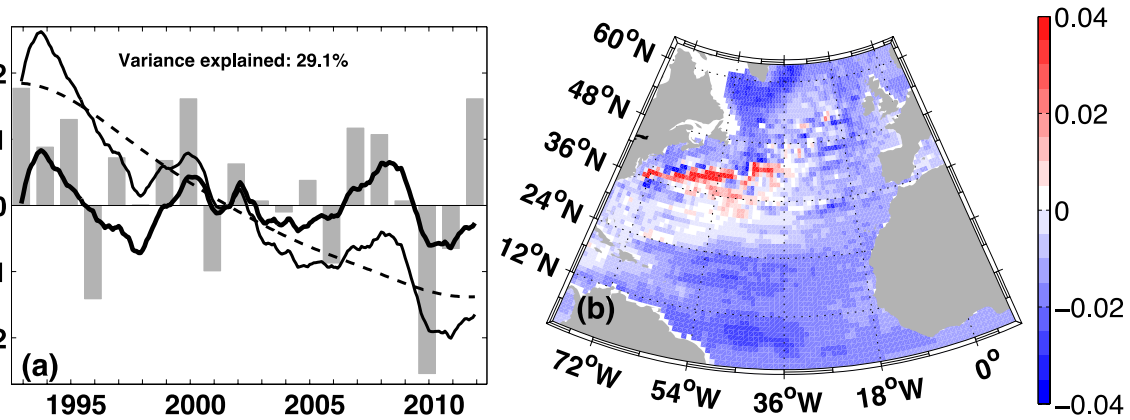


Figure 9. The subpolar gyre index: (a) The time series of the PC1 of the Aviso sea level anomalies (thin curve), and the time series with its nonlinear trend (dashed curve) removed (thick curve), overlapped by NAO index from December to March (grey bars) (a) and the associated EOF1 on $1^{\circ} \times 1^{\circ}$ grids (b).

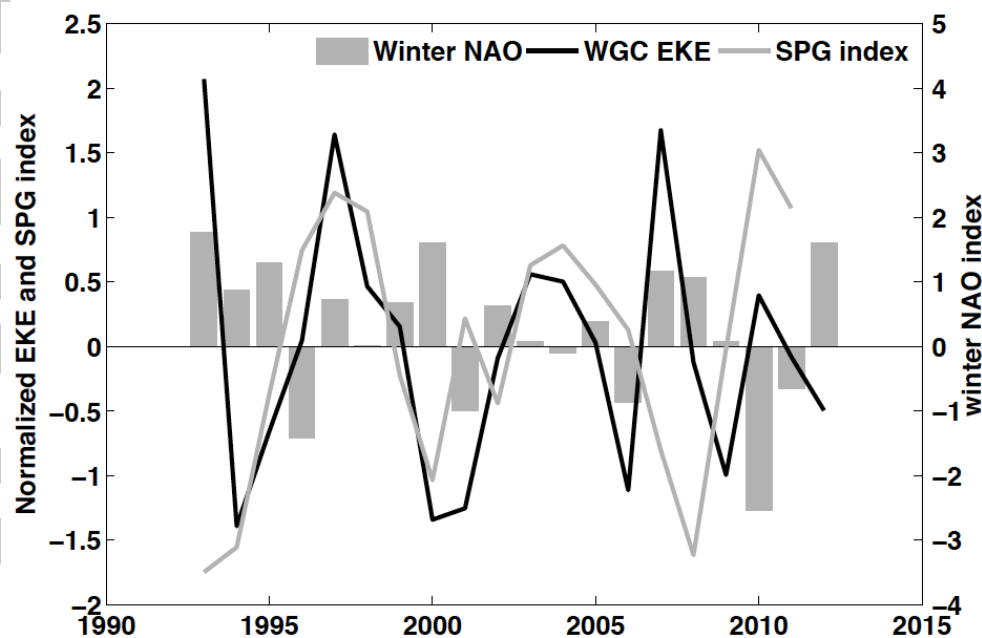


Figure 10. Time evolution from 1993 to 2012 for the normalized WGC EKE (black curve, unit: cm^2/s^2), the nonlinearly detrended and normalized September to December SPG index timed by -100 (grey curve), and the December to March NAO index timed by 30 (grey bars).

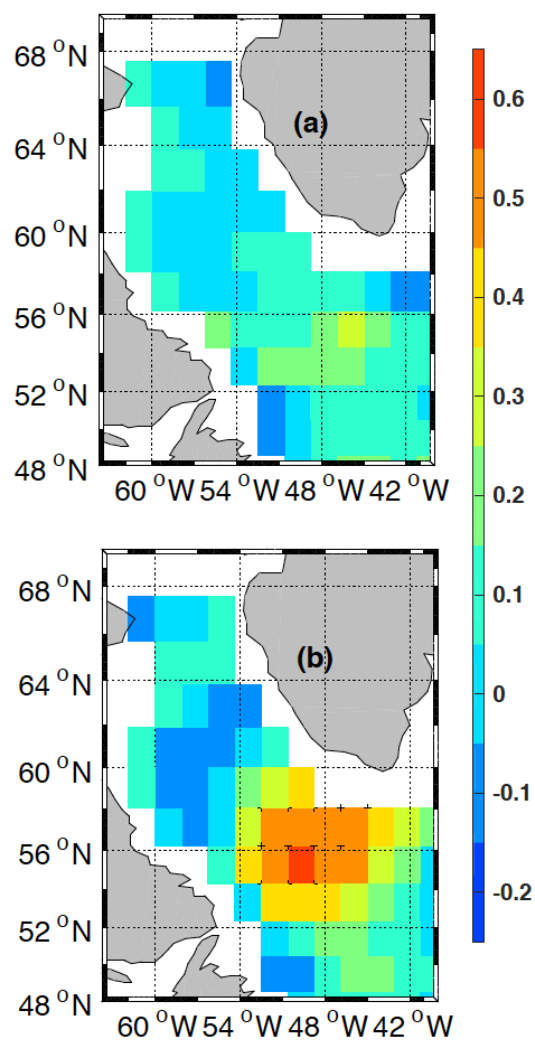


Figure 11. The correlation coefficient of (a) the WGC EKE and (b) the central Labrador Sea EKE from January to May with the NCEP reanalysis2 annual wind stress curl averaged from January to May. The stippling indicates confidence level above 95%.